NASA
Technical
Paper
2152

May 1983

Failure Mechanics in Low-Velocity Impacts on Thin Composite Plates

Wolf Elber

25
25th Anniversary
1958-1983

NASA

NASA Technical Paper 2152

1983

Failure Mechanics in Low-Velocity Impacts on Thin Composite Plates

Wolf Elber
Langley Research Center
Hampton, Virginia

National Aeronautics and Space Administration

Scientific and Technical Information Branch

Use of trade names or names of manufacturers in this report does not constitute an official endorsement of such products or manufacturers, either expressed or implied, by the National Aeronautics and Space Administration.

SUMMARY

Eight-ply quasi-isotropic composite plates of Thornel 300 graphite in Narmco 5208 epoxy resin (T300/5208)[1] were tested to establish the degree of equivalence between low-velocity impact and static testing. Both the deformation and failure mechanics under impact were representable by static indentation tests.

Under low-velocity impacts, such as tool drops, the dominant deformation mode of the plates was the first, or static, mode. Higher modes are excited on contact, but they decay significantly by the time the first-mode load reaches a maximum.

The delamination patterns were observed by X-ray analysis. The areas of maximum delamination coincided with the areas of highest peel stresses. The extent of delamination was similar for static and impact tests.

Fiber failure damage was established by tensile tests on small fiber bundles obtained by deplying test specimens. The onset of fiber damage was in internal plies near the lower surface of the plates. The distribution and amount of fiber damage were similar for impact and static tests.

INTRODUCTION

The impact resistance of graphite-epoxy composites is much lower than that of aluminum. Also, because these composites lack ductility, the damage is often not visible from the impact side. In aluminum aircraft structures, the denting from mild impacts has not posed a serious problem in the past, so the problem has not been studied extensively. Consequently, neither the impact deformation mechanics nor the failure mechanics for low-velocity impacts are well enough understood to explain the behavior of composites or to predict the influence of varying the matrix or the fibers on their impact behavior. Reference 1 and this study are part of a concerted effort at NASA Langley Research Center to quantify the impact mechanics under low-velocity impacts and to produce superior composites with improved impact resistance.

If a hard object strikes a composite plate, it should, after temporarily converting all impact energy into strain energy, rebound without causing significant damage. For elastic materials, there must be a family of impact events characterized by low impact velocities and high object masses. For such a family, the deformation mechanics are essentially equivalent to the deformation mechanics under quasi-static loading. If this family encompasses common impact conditions and covers cases up to the level of significant damage, then a large fraction of impact problems can be studied through inexpensive quasi-static tests and simple analyses.

The objective of this study was to establish the degree of equivalence between impact tests and similar static tests for thin 8-ply graphite-epoxy plates with a quasi-isotropic $[0/45/-45/90]_S$ stacking sequence. A 25-mm-diameter steel ball was chosen as the lightest object characteristic of tool-drop problems. If impacts with

---

[1] Thornel: Registered trademark of Union Carbide Corporation. Narmco: Registered trademark of Narmco Materials Division, Whittaker Corporation.

that ball are equivalent to the static test, then all impacts from heavier objects should correlate even better with static tests at similar energies.

The equivalence of deformation mechanics was examined by comparing load displacement records for the two test types, matrix damage and fiber damage. Matrix damage was established by X-ray analysis, and fiber damage was established by deplying the test plates and testing narrow fiber bundles in tension.

EXPERIMENTAL PROCEDURE

Impact Tester

Figure 1 schematically shows an impact tester consisting of a 25-mm-diameter steel-ball impactor mounted on a fiberglass cantilever. The ball carried a 20 000g accelerometer with the signal lines bonded to the cantilever. The specimen plane was located at the level where the cantilever is unstressed. The cantilever length was 75 cm and the flexural stiffness was 50.1 N-m, measured at the impact center of the ball.

The impactor was raised to a fixed height h and was released. After the impact, the cantilever was caught to avoid multiple impacts. The impact velocity V_o has been measured and is within 2 percent of the velocity calculated from total-energy considerations. That is,

$$V_o = \sqrt{2(kh^2/2 + Mgh)/M}$$

where

k flexural stiffness of cantilever, 50.1 N-m

g gravitational acceleration, 9.8 m/s^2

M effective mass of ball and cantilever, 0.113 kg

This simple device produced impact velocities up to 7 m/s, or impact energies of 2.7 J.

Data Reduction

The acceleration history a_t was digitally stored in an oscilloscope. Using double integration from the moment of contact at velocity V_o, the velocity history V_t of the ball and plate is

$$V_o + \int a_t \, dt$$

where t is time, and the displacement history δ_t is

$$\int V_t \, dt$$

The load P_t transmitted between plate and ball was the product of the acceleration and the mass of the ball. Load-displacement records can thereby be obtained from the accelerometer data.

X-Ray Delamination Determination

A zinc iodide solution was used as an X-ray opaque filler on all specimens. On most dynamic tests, the solution was applied to the front and back surfaces of the impact specimens after the test. Capillary forces then dispersed the solution into the delamination cavities. In many specimens air pockets remain inside the larger cavities. In the static tests a film of zinc iodide solution was applied to the backface of the specimens before the tests to avoid air penetration into the cavities. This method was somewhat superior to applying the solution after the test. However, the overall extent of delamination measurements is not affected by the air pockets, which typically form near the center of the indentation.

Fiber Bundle Strength Determination

Graphite-epoxy specimens were thermally deplied. The best results, with respect to ply flatness and matrix degradation, were obtained by laying the laminate between two sheets of 2-mm-thick aluminum alloy to maintain flatness. This sandwich was then wrapped in aluminum foil to exclude most of the oxygen. The outgassing of the matrix inside this package was assumed to produce an essentially inert environment. The laminate was heated in a laboratory oven at 648 K for about 1 hour.

The laminate was separated into individual laminae after cooling. In some instances, a razor blade was required to obtain a clean separation. The center of impact had been surveyed relative to the four corners of the rectangular laminate and could be reestablished on each individual lamina. A 10-mm-wide strip, centered around the impact location, was then "stripped" out of the lamina. This stripping is relatively simple because the deplying process tends to produce natural segregation into units approximately equal to the original tows.

The 10-mm strips were then subdivided into about 10 approximately equal "tows," each approximately 1 mm wide. Again, a razor blade was sometimes used in this splitting operation. The blade follows the twist of the tows so that minimal fiber damage is produced.

Before stripping, the original laminate density was obtained from the weight of the laminate, the rectangular dimensions of the laminate, and the average ply thickness of the cured laminate.

The cross-sectional area (with matrix) of each strip was then calculated from the weight of the strip, the length of the strip (the only measurable dimension), and the laminate density.

Tension specimens were fabricated by bonding the ends of each strip between two 25-mm-square aluminum platelets (1 mm thick) with an epoxy film adhesive. These specimen end tabs were cured in curing frames for 1 hour at 393 K. The gage length of these tension specimens was 50 mm.

The tensile tests were conducted in a table-top screw-driven tension tester. Strengths were computed from the maximum load and the computed cross-sectional area.

The coordinate of each strip was defined as the distance of the center of the strip from the impact center. Residual strengths are presented as a function of this distance from the center of impact.

RESULTS AND DISCUSSION

Deformation Mechanics

Static tests.- The large deformation solution for a clamped circular plate was developed in reference 1. For comparison with the impact tests or 50-mm-diameter plates, several static tests in which both displacements and lower surface strains were measured were repeated on similar plates. Eight-ply quasi-isotropic composite plates of Thornel 300 graphite in Narmco 5208 epoxy resin (T300/5208) were used for these tests. Figure 2 is the load-displacement relation for a plate subjected to a load cycle of 90 percent of the average penetration load. As found previously, the load-displacement curve follows very closely the large deformation laminate predictions (dash-dot curve). Also, after the onset of delamination the load-displacement curve tends toward the dashed curve, which represents a totally delaminated membrane. The unloading curve has a curvature similar to the membrane curve. This similarity indicates that the cracked plate is dominated by the membrane stretching behavior.

For the same configuration, figure 3 shows the strain-gage response, over a 1-mm gage length directly under the load point, as a function of displacement. The results from four tests show that, up to the displacement where delamination starts (1.0 mm), the measured strains agree fairly well with the predicted results for large deformation analysis. However, once ply splits develop under the strain gages, large scatter in the strain measurements results. In fact, several specimens had indicated strains above 16 ms, far beyond the strain capability of the T300 fiber. In the section entitled "Failure Mechanics," it is shown that the outer ply has no significant fiber damage. It appears, therefore, that the resistance strain gages provide unreliable results above the splitting loads.

Impact tests.- A number of impact tests were conducted on specimens from the same composite plate from which the static specimens were taken. The first objective was to establish the degree of equivalence in deformation mechanics between the low-velocity impact tests and the static tests. This is accomplished by comparing the load and displacement histories.

Figure 4 shows the acceleration trace from an impact test at 0.61 J energy, scaled to impact load. Figure 5 shows the corresponding displacement trace obtained by double integration of the acceleration trace. The force trace consists essentially of the first mode of plate deformation, as indicated by the dashed line representing the appropriate analysis. The higher modes of vibration visible in the force trace have decayed to negligible amplitude near the maximum load. The displacement trace shows no visible higher modes. The residual displacement of about 10 percent of the maximum displacement is similar to values obtained in static tests. The first mode analysis, of course, does not model any residual displacements, as is seen from the dashed line. The constants used in the analysis are listed in table I. The large deformation analysis for plates with significant shear deformations was taken from reference 1.

TABLE I.- CONSTANTS FOR ANALYSIS

Plate radius, mm	25.4
Plate thickness, mm	1.04
Indentation constant, $MN\text{-}m^{-3/2}$	250
Shear modulus, GPa	2.5
Flexural modulus, GPa	54
Ball radius, mm	12.7
Ball mass, g	113
Composite density, Mg/m^3	1.45

To analyze the higher modes and the large initial loading rate, a simple dynamic model of the impact system was analyzed. Figure 6 shows a two-degree-of-freedom model in which the indentation stiffness of the plate is a massless nonlinear hysteretic spring and is coupled to the plate through the effective mass of the plate. The plate stiffness was further substructured into shear stiffness and flexural stiffness in parallel with a nonlinear spring that represents the membrane. A dynamic analysis of that model produced the load trace shown by the dashed line in figure 7. The behavior is very similar to the test-load trace represented by the solid line.

Examination of the model shows that the dominant higher mode is the first mode of vibration of the flexural plate without the ball mass. This mode vibrates 180° out of phase with the shear and indentation spring. The decay of amplitude in the second and third cycles and the consequent increase in amplitude in the fourth and fifth cycles cannot be modeled and are obviously relatable to energy released by the damage process.

Figure 8 shows the indentation hysteresis loop produced by the indentation functions used in the model. These functions have the form suggested in reference 2, with Hertzian loading and cubic unloading. Figure 9 shows the displacement trace obtained in the dynamic analysis. It also is similar to both the test data and the first mode analysis.

The analysis shows that the first mode analysis of plate deformation mechanics is sufficiently accurate to determine impact loads and displacements in thin plates. The higher modes appearing early in the test should be of greater significance in thick plates, where the mass of the plate is of the order of the mass of the impactor.

Failure Mechanics

Matrix damage.- The delamination and matrix cracking parallel to the fibers (ply splitting) were observed in both impact and static tests at various maximum energy levels.

In all cases, splitting of the lowest ply was the first visible (external) damage, and it occurred at the loads at which the strain measurements began to become erratic. Figure 10 shows delamination X rays of four separate specimens after they had been loaded as indicated. The load-displacement trace was taken from the specimen with the highest load. The two dominant cracks in the 8th ply formed first. Delamination between plies 7 and 8 surrounded these two cracks. Ply cracks in

ply 7 formed next. Delamination is visible as a light-gray shadow. The darkness of the shadow indicates the thickness of the dye-penetrant layer, hence the separation between the plies. No delamination appears directly under the impact center, because that is the area of zero shear and compressive interlayer stresses. The predominant growth of delamination is in the direction of the 8th ply.

Figure 11 shows a similar sequence of X rays from four impact specimens tested to four energy levels. The maximum loads in each test are indicated on the load-displacement trace for the specimen impacted with the highest energy. The progression of damage is similar, with the dominant ply-splitting direction being in the 8th ply.

Both the static tests and the impact tests show that the delamination and ply cracking propagate furthest in the bottom ply in the fiber direction. A full mathematical analysis for the deformation and failure mechanics does not exist yet, but a three-dimensional visualization of these mechanics is given here.

The lower plies dominate the failure mechanics of the plate under a transverse point load. Figure 12 is an isometric view of three fiber strips, the 8th ply center strip running under the load point parallel to section A-A, the 7th ply center strip, 45° to the bottom ply, running parallel to section B-B, and an off-center strip in the 8th ply. Under the large-plate deformation existing during the delamination, the center strip in the 8th ply carries high membrane stresses. As shown in section A-A of figure 13, the shape of that strip in the laminated plate has a strong upward concave curvature and is maintained at that curvature by tensile peel stresses between the 7th and 8th plies. A large fraction of the strain energy in the 8th ply is shed during the delamination. As a result, the trajectory of that ply is virtually a straight line between the load point and the support. This result is also shown in section A-A of figure 13.

The center strip in the 7th ply is restrained from straightening in a similar fashion by the support from off-center strips in the 8th ply. This is shown schematically in section B-B of figure 13. If the matrix action is ignored, the deformation of this multistrip trampoline shows that the 7th ply can shed only a small fraction of its strain energy.

The model shown in figure 14 was constructed to help visualize the interply separation in the delaminated state. The model consisted of four layers of 2-mm-thick plexiglass strips and one 8-mm-thick sheet, all bonded together outside the circular area. The strips of the 8th ply run vertically in the photograph. This represents a composite impact specimen in which ply cracks and delaminations have progressed to the supports. The model was deformed into the deflected shape with a 25-mm-diameter steel ball. The delamination cavities were then filled with dye for the transmission photograph shown.

Because of the tendency of the dye to run downward from the deformation dome, large air bubbles formed between the 7th ply and the center strip of the 8th ply. That was the area of largest interply separation. Perpendicular to ply 8, along the direction of ply 5, is the area of least dye content. In that area the off-center strips in the 8th ply are loaded. Therefore, that area has compressive interply stresses throughout the thickness.

The air bubble pointing from the load center in the indicated direction of the 7th ply outlines the area of tensile peel separation between plies 6 and 7. This area is much smaller than the area between plies 7 and 8.

The X-ray delamination determination revealed delamination patterns very similar to the peel separation pattern obtained from this model. Because the shear-stress distribution in the vicinity of the load center is essentially axisymmetrical and the delamination pattern is oriented in the direction of tensile peel stresses, the conclusion can be drawn that the delamination progression is dominated by the low peel strength of the matrix material rather than by the shear strength. The maximum delamination lengths from static and impact tests are summarized in figure 15. The results indicate that at all energy levels the delamination length in the static tests is somewhat greater than in the impact tests. But from an engineering viewpoint the delamination damage can be considered equivalent.

Other investigators (ref. 3) have found that "stitching" of the laminate decreases delamination. That is logical if delamination is, in fact, driven by peel delamination. Stitching has a greater restraining effect on peeling than on shear delamination. Similarly, tests showed that a woven ply on the back of the laminate delaminates less than two crossed laminae. This also is explainable because the weave does not allow one free strand to peel free without involving cross-ply strands.

Fiber damage.- Two impact specimens and one static-load specimen were examined for fiber damage with the deplying-bundle testing technique. This type of bundle test provided strengths comparable to the original lamina strength and, hence, provided a good estimate of the percentage of fibers broken in a bundle. The method is superior to photomicroscopic examination, because microscopy only reveals damage on the surface and provides less quantitative information.

Figure 16 shows the residual bundle strength distribution for a specimen loaded statically to a strain energy of 0.92 J. Figure 16(a) shows the strengths for plies 6, 7, and 8. Plies 4 and 5, the parallel symmetry plies, were nonseparable and were tested together. Figure 16(b) shows these data together with data for plies 2 and 3. Ply 1 is not shown.

The data for ply 6 show that two strips near the impact center were almost completely broken. That damage was visible to the naked eye. Far from the load center the bundles have a baseline strength of 1.26 GPa with a 10-percent coefficient of variation.

The data for ply 7 show two test points near the load center with a reduction of 30 to 50 percent in strength below the average remote strength. Such damage is not usually visible to the naked eye, and is only rarely found under an optical microscope.

The data for ply 8 show two minima. Although these two data points are statistically not significant, the pattern of two minima around the load center has occurred in other specimens. A more extensive statistical study is needed to establish whether fiber damage in some plies does in fact start in an area outside the load center.

In figure 16(b), plies 4 and 5 show significant damage on one side of the load center and a small amount of damage on the other side of the load center. Plies 2 and 3 show no damage. Ply 1 also showed no damage and, to retain clarity, was not plotted.

To quantify the damage in each ply, an equivalent-damage width for each ply was calculated from the integral of the strength reduction below the remote ply strength.

Figure 17 shows the equivalent damage width for each ply. The damage in plies 4 and 5 was wholly attributed to ply 5, based on observation of the failure mode. The maximum damage width of 4 mm occurs for ply 6.

The first impact specimen was tested for residual bundle strength to an energy of 0.61 J, an estimated threshold for fiber damage. (See fig. 18.) Because of excessive deplying temperature, all bundles showed a relatively uniform reduction in strength, but as a function of impact location, plies 5, 6, and 8 showed no local damage. Ply 7 shows the two strength minima around the impact center, and an equivalent damage width of 0.3 mm was calculated for that strength reduction.

Figure 19 shows the ply damage analysis for all 8 plies of an impact specimen tested at 1.04 J. In figure 19(a), all 4 lower plies show significant damage; the widest ply crack is in ply 7. In figure 19(b), all 4 upper plies show no significant damage near the impact center.

The equivalent-damage width for all three specimens is summarized in figure 20. It shows that the maximum damage in all cases is either in the 6th or 7th ply and that the amount of fiber damage grows monotonically with the energy of the test condition.

The total-damage width, the sum of the damage in each ply, is plotted in figure 21 as a function of loading energy. Compared with a straight-line interpolation between the two impact data points, the static-load test shows less fiber damage than the impact test. This is consistent with the fact that the static tests have slightly more matrix damage. The strain measurements shown in figure 3 indicate that, if no matrix damage occurs, fiber damage should occur when the strains reach 1.2 percent at an energy level of about 0.36 J. Ply cracking and delamination therefore reduce fiber strains, and less fiber damage is expected if more matrix damage occurs.

Figure 21 also shows the penetration energy for a 50-mm-diameter plate from reference 1. The first measurable fiber damage observed at 0.61 J occurs at about one third of the penetration energy. That penetration energy was found to be controlled only by fiber properties, provided that the matrix was brittle.

For the T300/5208 graphite-epoxy, the differences in damage mechanics between static and impact tests are small. Static tests and analysis are therefore useful tools for damage characterization.

CONCLUSIONS

Eight-ply quasi-isotropic composite plates of Thornel 300 graphite in Narmco 5208 epoxy resin (T300/5208) were tested to establish the degree of equivalence between low-velocity impact and static testing. The study resulted in the following conclusions:

1. For thin composite plates, the deformation mechanics of low-velocity impact tests and static tests are sufficiently equivalent to allow static testing for material screening tests. Higher modes of vibration are related to indentation vibrations and have little effect on the maxima of displacements and loads.

2. For the similar plates the failure mechanics are sufficiently equivalent to use static tests for the assessment of impact damage and to screen materials.

3. The matrix damage was concentrated in areas where kinematic considerations indicate high interlaminar peel stresses rather than in areas of high shear stresses.

4. The fiber damage was most severe in the plies just inside the back surface of the plates, where the strains are highest in the presence of delamination.

Langley Research Center
National Aeronautics and Space Administration
Hampton, VA 23665
April 12, 1983

REFERENCES

1. Bostaph, Gretchen M.; and Elber, Wolf: Static Indentation Tests on Composite Plates for Impact Susceptibility Evaluation. Proceedings of the Army Symposium on Solid Mechanics, 1982 - Critical Mechanics Problems in Systems Design, AMMRC MS 82-4, U.S. Army, Sept. 1982, pp. 288-317.

2. Sun, C. T.; and Chattopadhyay, S.: Dynamic Response of Anisotropic Laminated Plates Under Initial Stress to Impact of a Mass. AFML-TR-74-258, U.S. Air Force, Mar. 1976. (Available from DTIC as AD A025 906.)

3. Williams, Jerry G.; and Rhodes, Marvin D.: The Effect of Resin on the Impact Damage Tolerance of Graphite-Epoxy Laminates. NASA TM-83213, 1981.

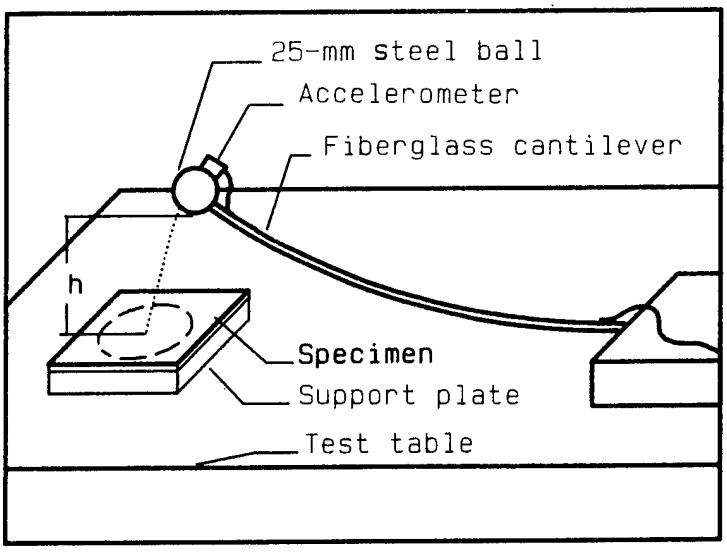

Figure 1.- Schematic of cantilever impact fixture.

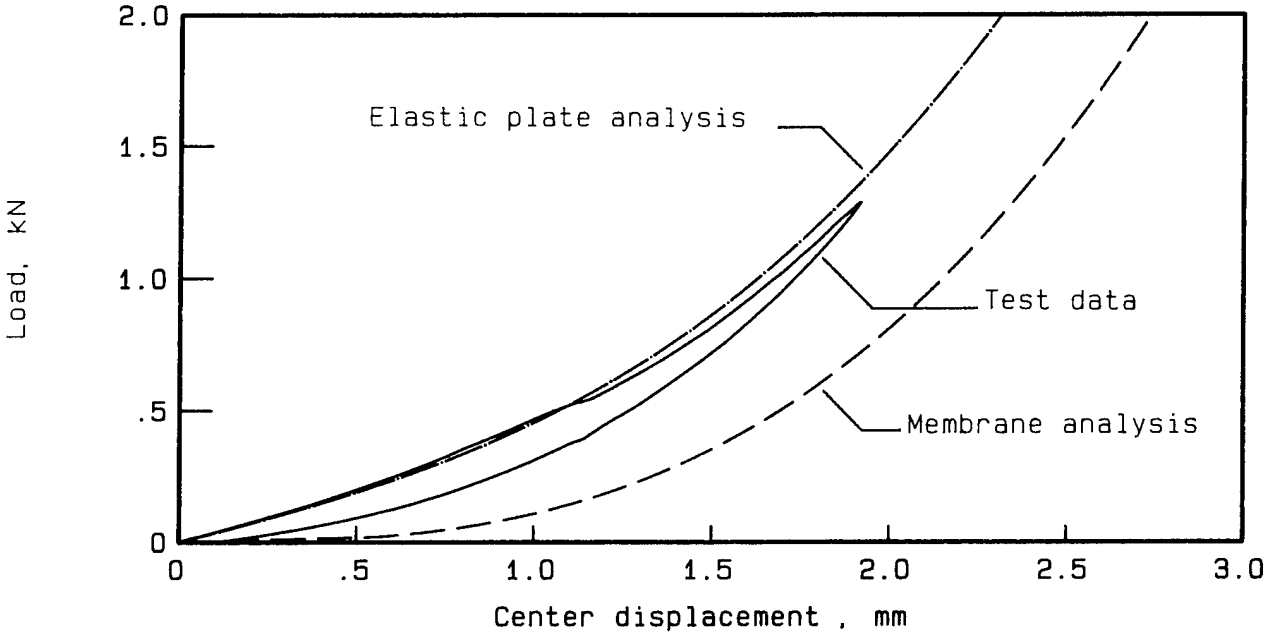

Figure 2.- Load-displacement relation for a 50-mm-diameter 8-ply quasi-isotropic plate (T300/5208).

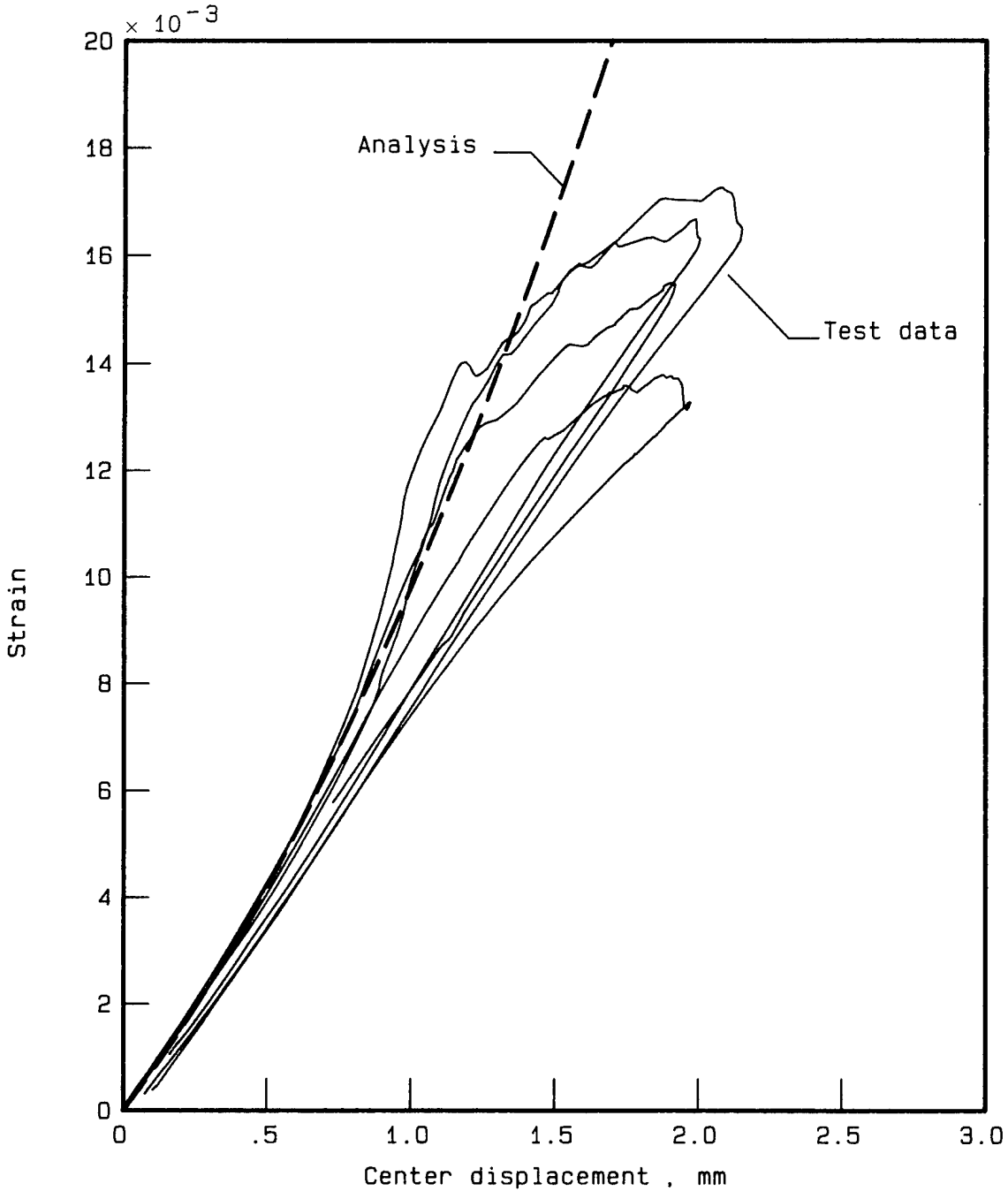

Figure 3.- Lower-surface fiber strain as a function of displacement for four 50-mm-diameter 8-ply plates.

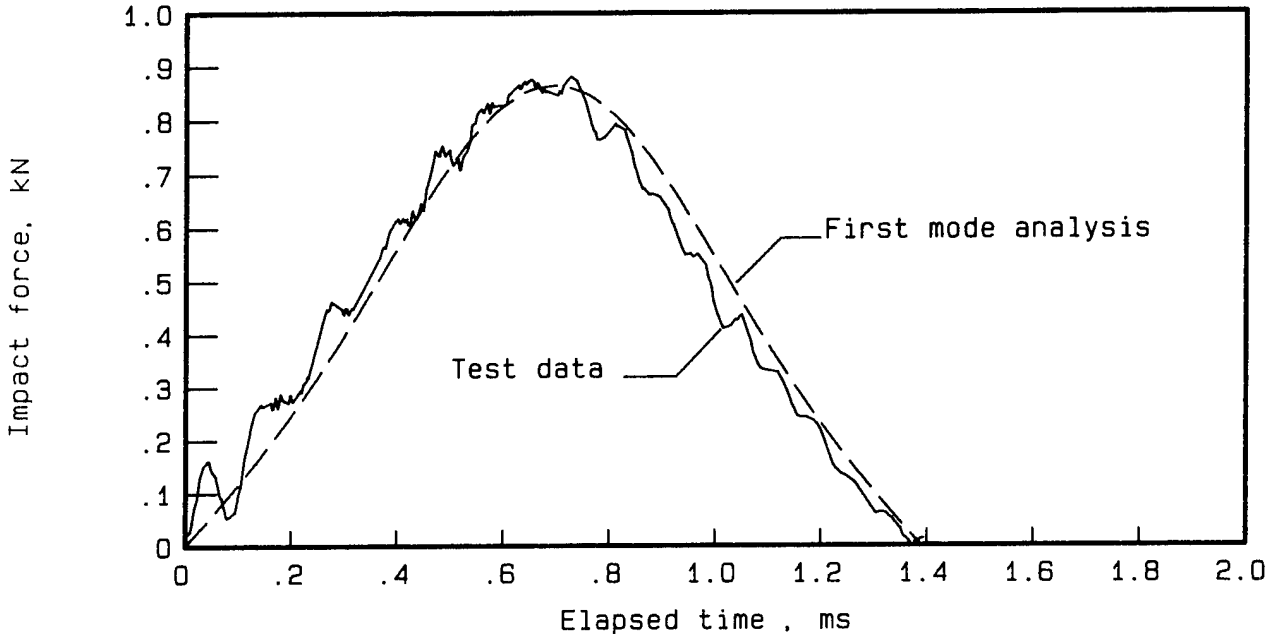

Figure 4.- Impact force trace for impact energy of 0.61 J.

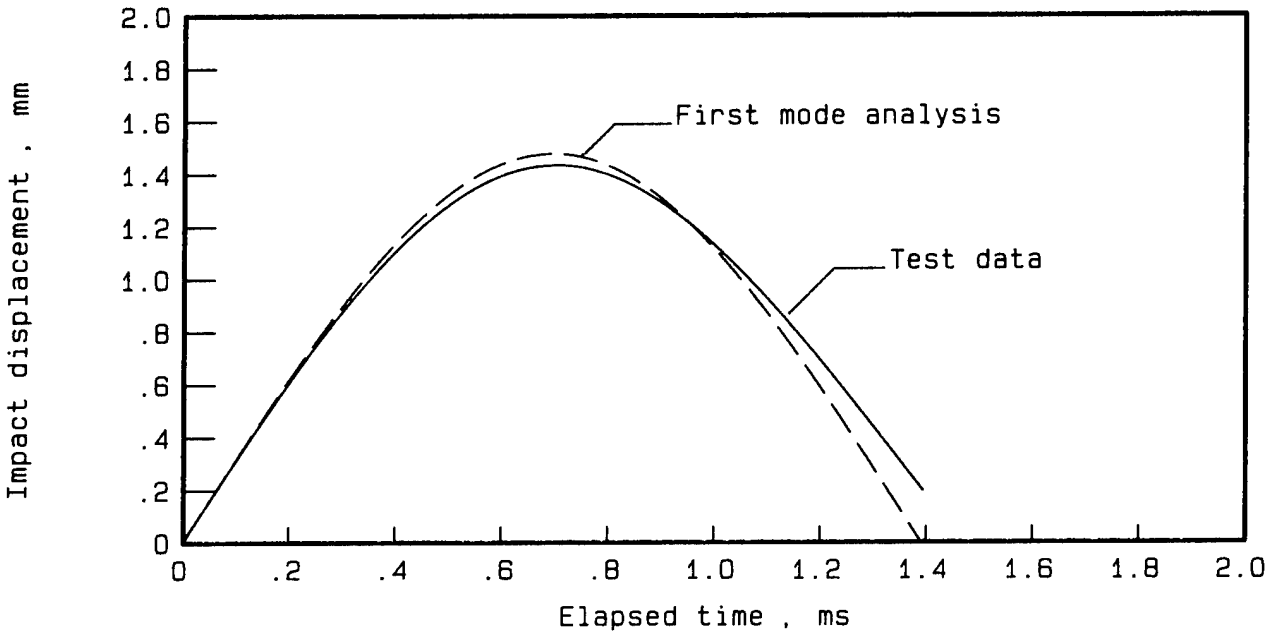

Figure 5.- Impact displacement trace for impact energy of 0.61 J for a 50-mm-diameter 8-ply plate.

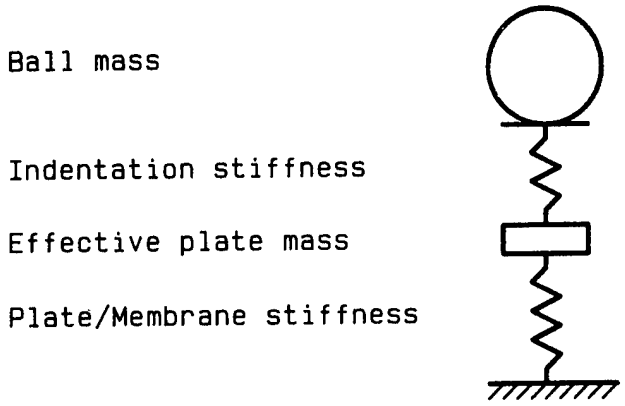

Figure 6.- Two-degree-of-freedom model for impact on a thin plate.

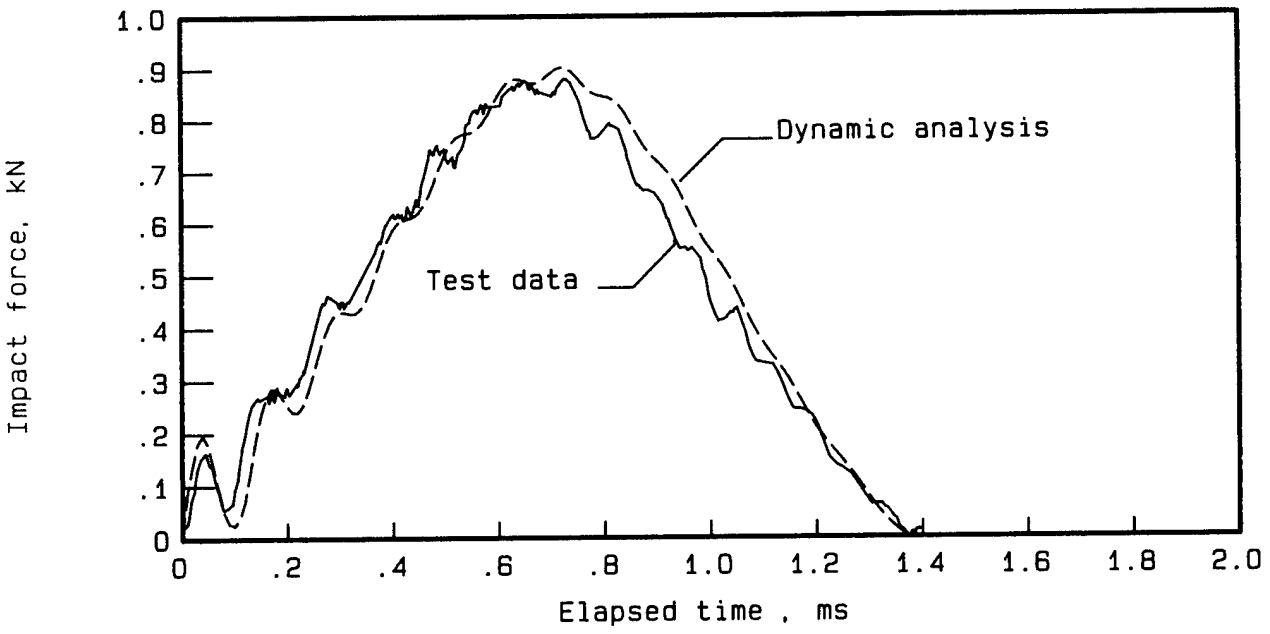

Figure 7.- Impact force trace for impact energy of 0.61 J from both test and analysis.

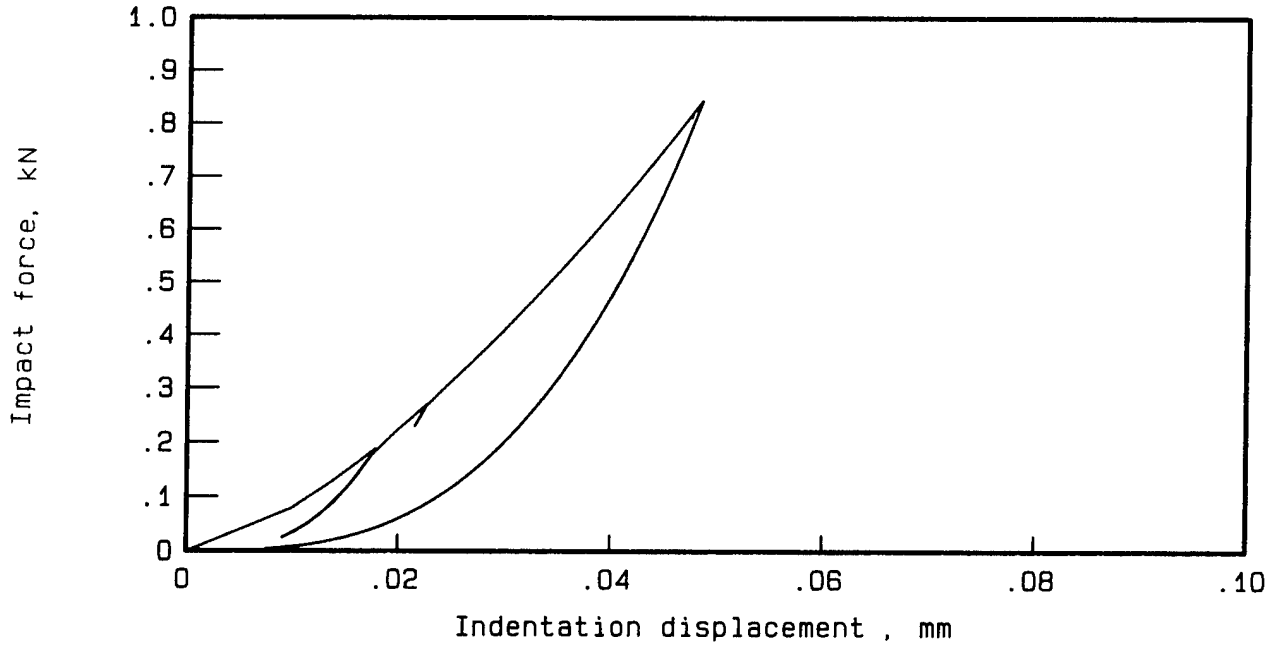

Figure 8.- Analytical indentation hysteresis loop for impact of 0.61 J.

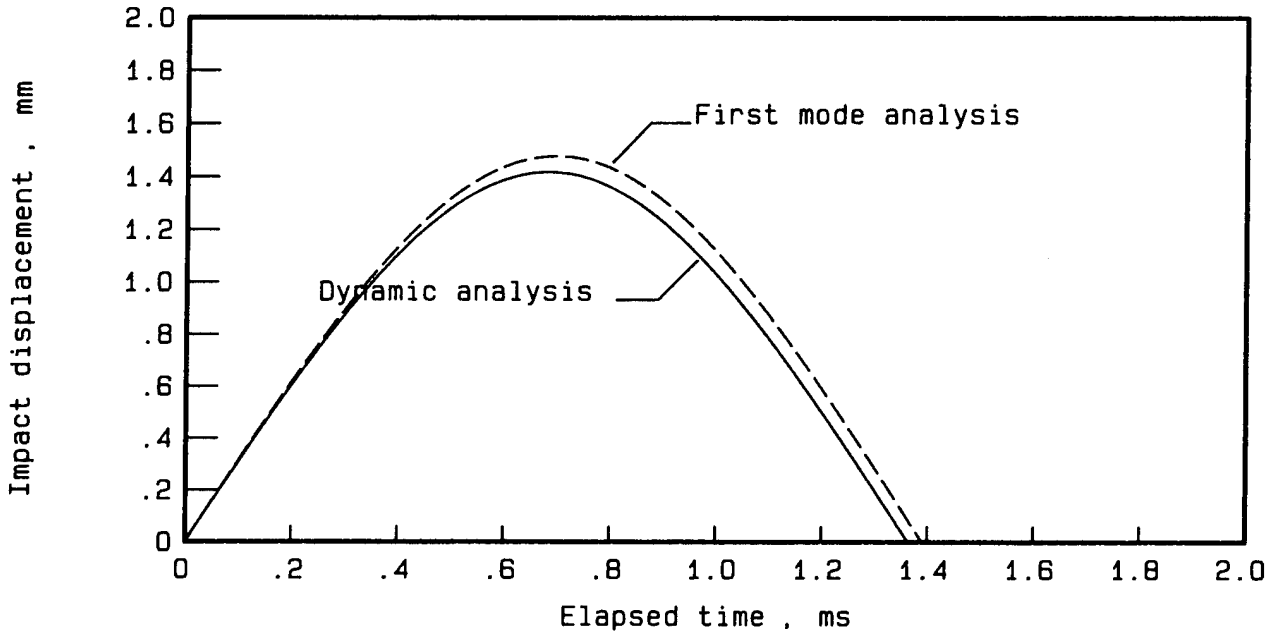

Figure 9.- Comparison of displacement traces for first mode and dynamic analyses.

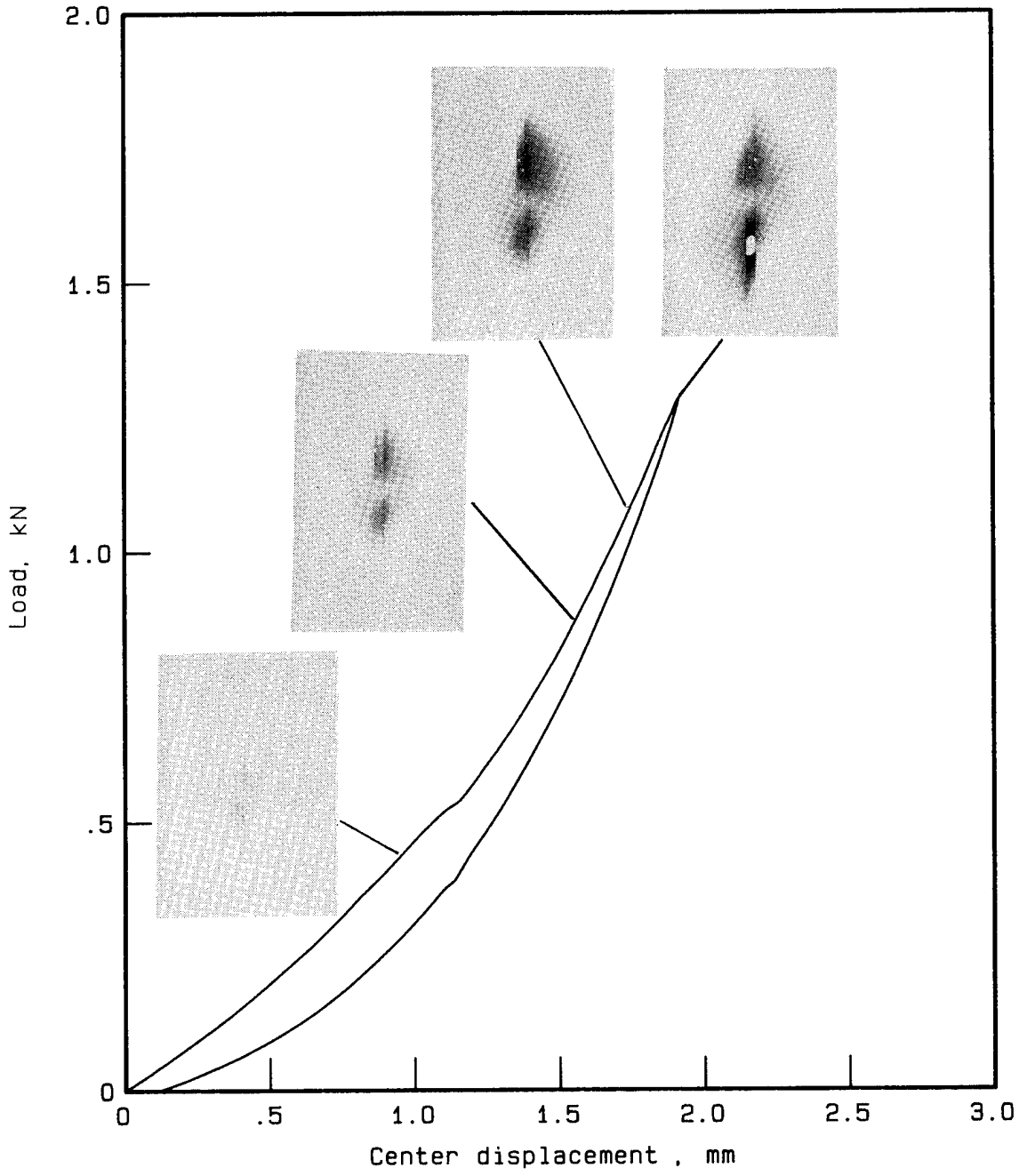

Figure 10.- X-ray delamination analysis for static test conditions.

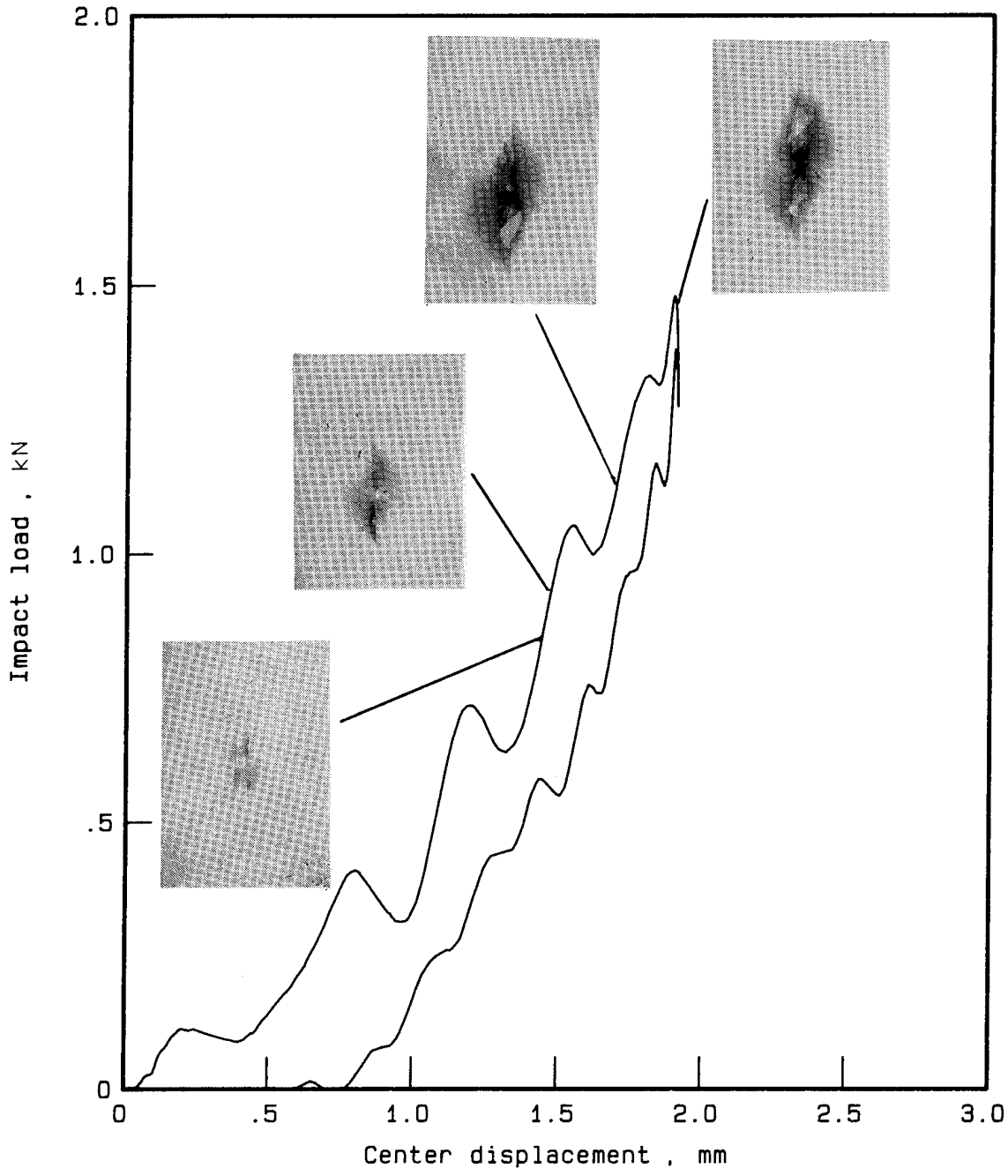

Figure 11.- X-ray delamination analysis for impact test conditions.

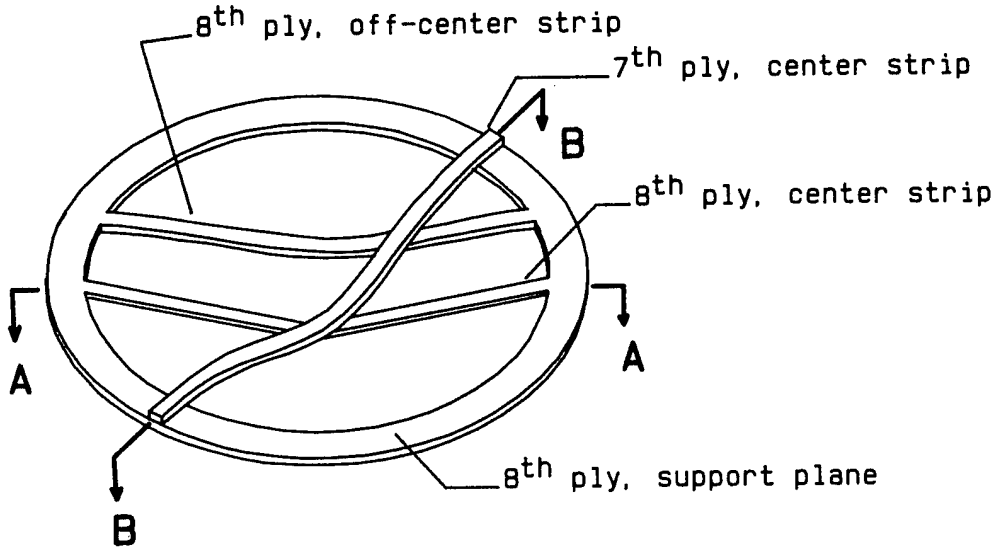

Figure 12.- Schematic of deformations of two lowest plies.

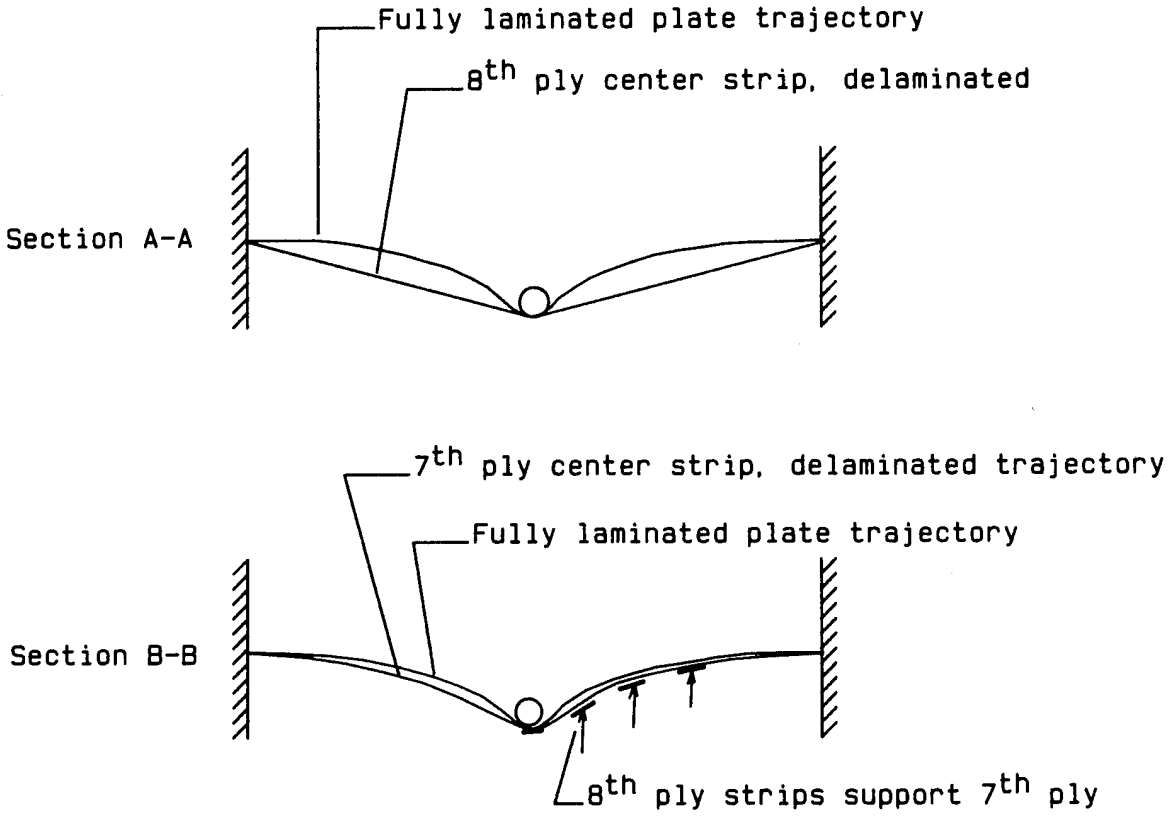

Figure 13.- Sections A-A and B-B of plate strips in figure 12.

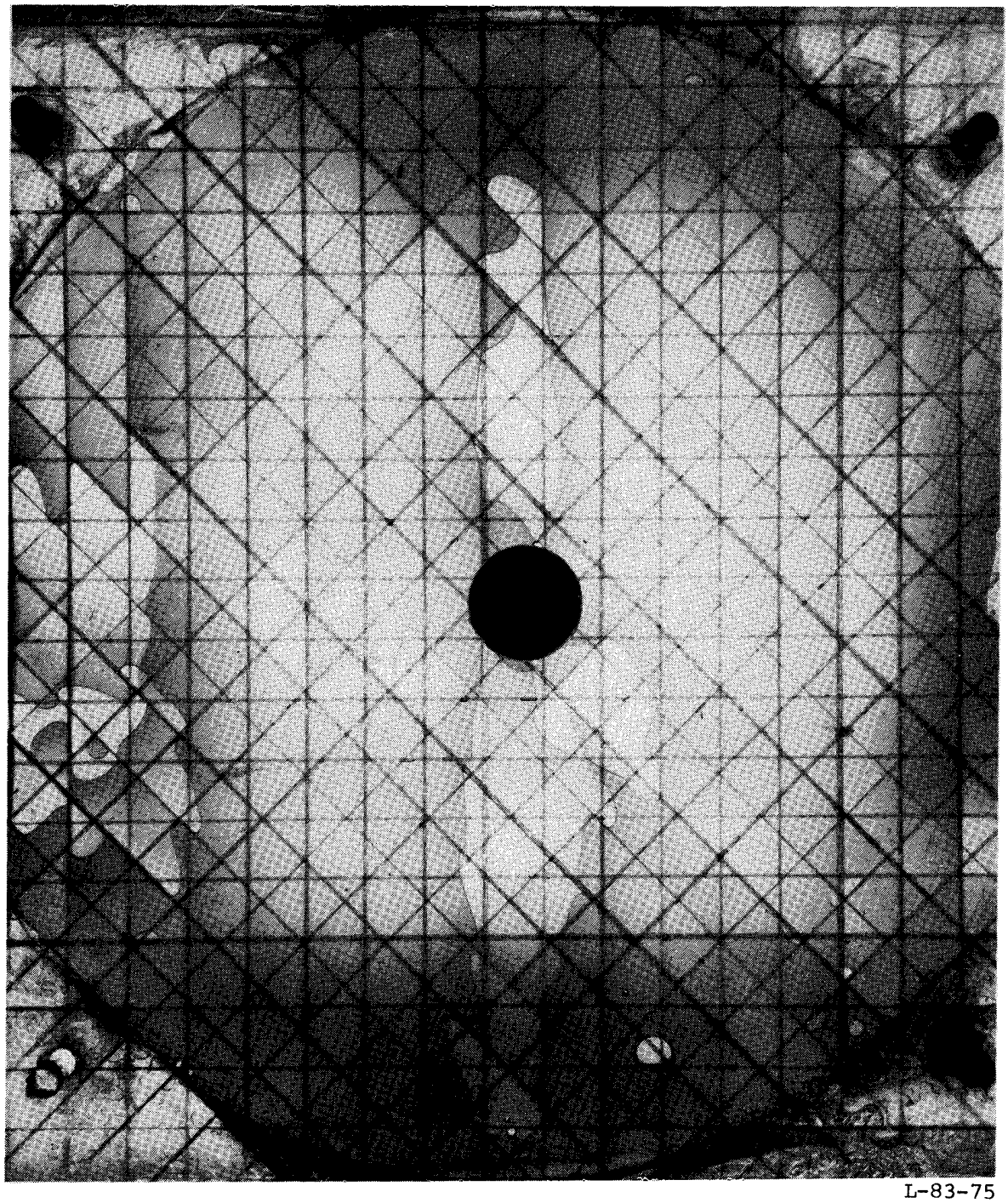

L-83-75

Figure 14.- Transmission photograph of a plastic strip model of a laminate under impact. Dark tone represents delamination.

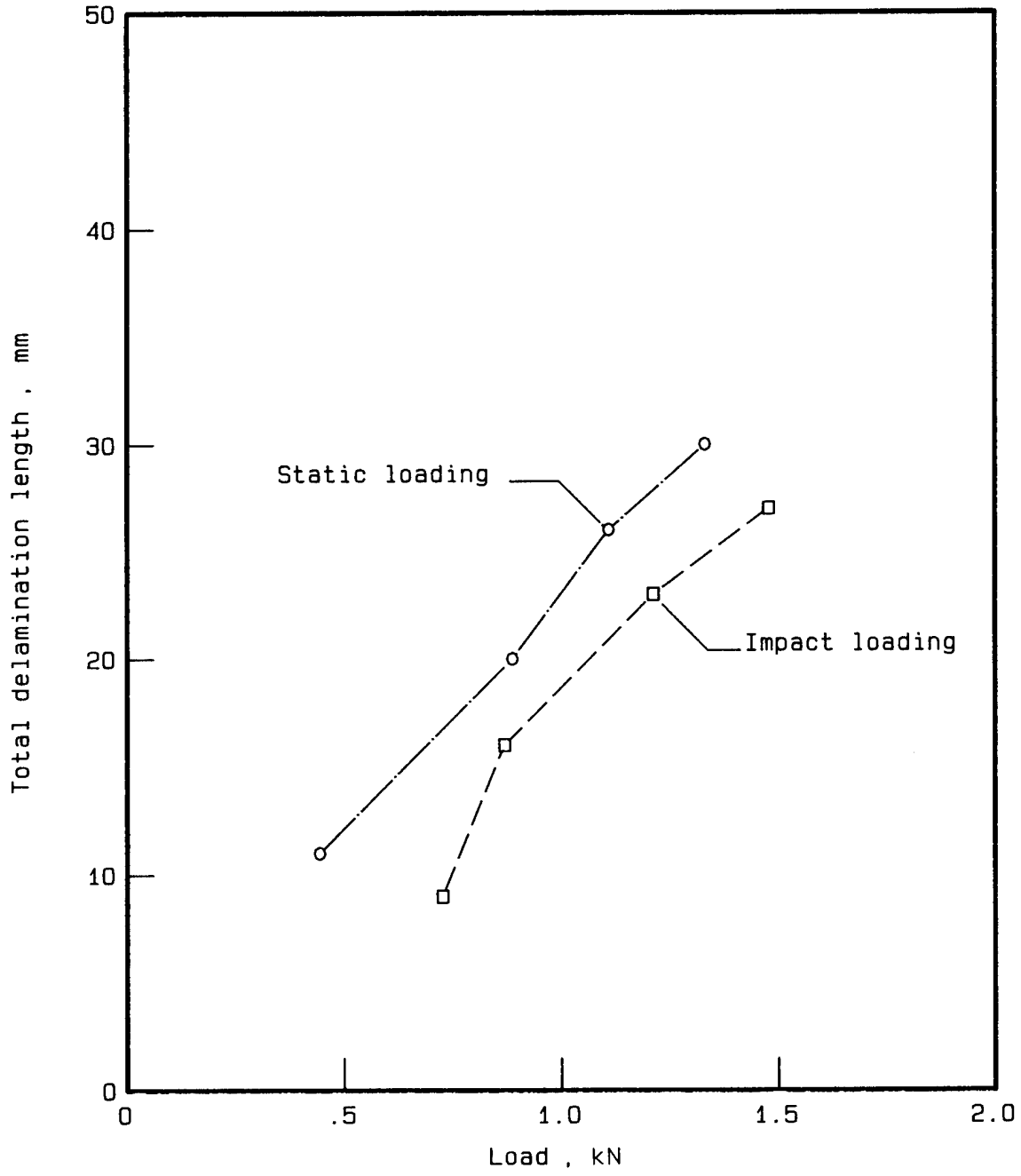

Figure 15.- Comparison of delamination under impact loading with delamination under static loading.

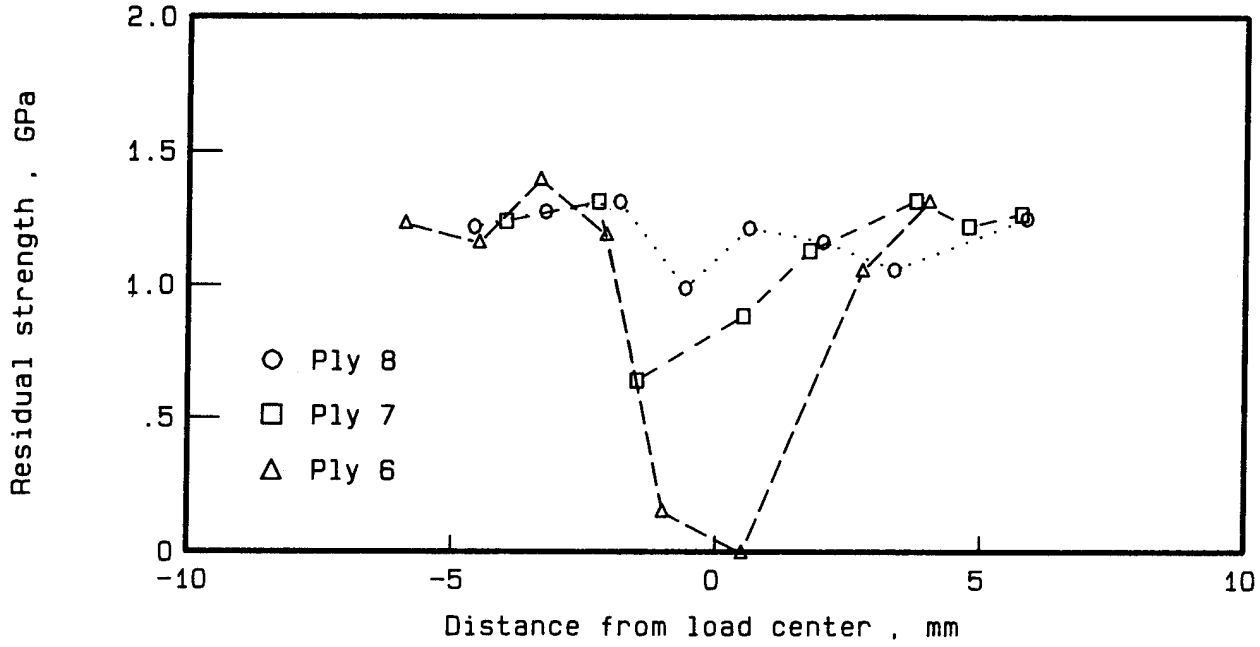

(a) Plies 6, 7, and 8.

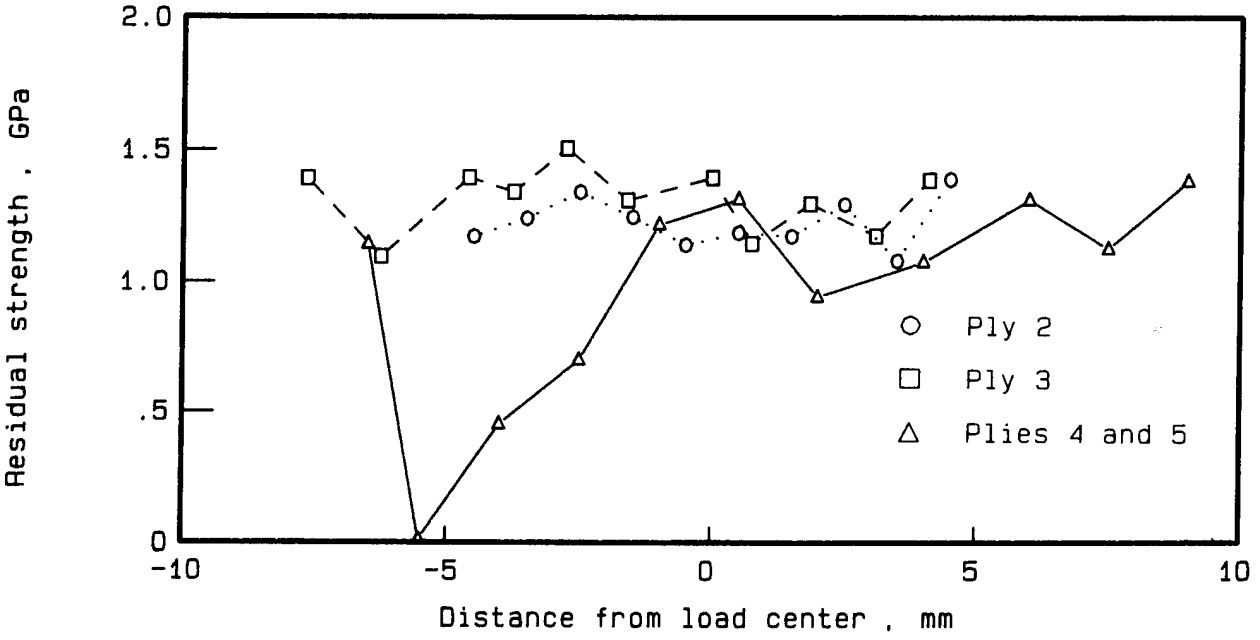

(b) Plies 2, 3, 4, and 5.

Figure 16.- Residual bundle strength analysis for a static load up to a strain energy of 0.92 J.

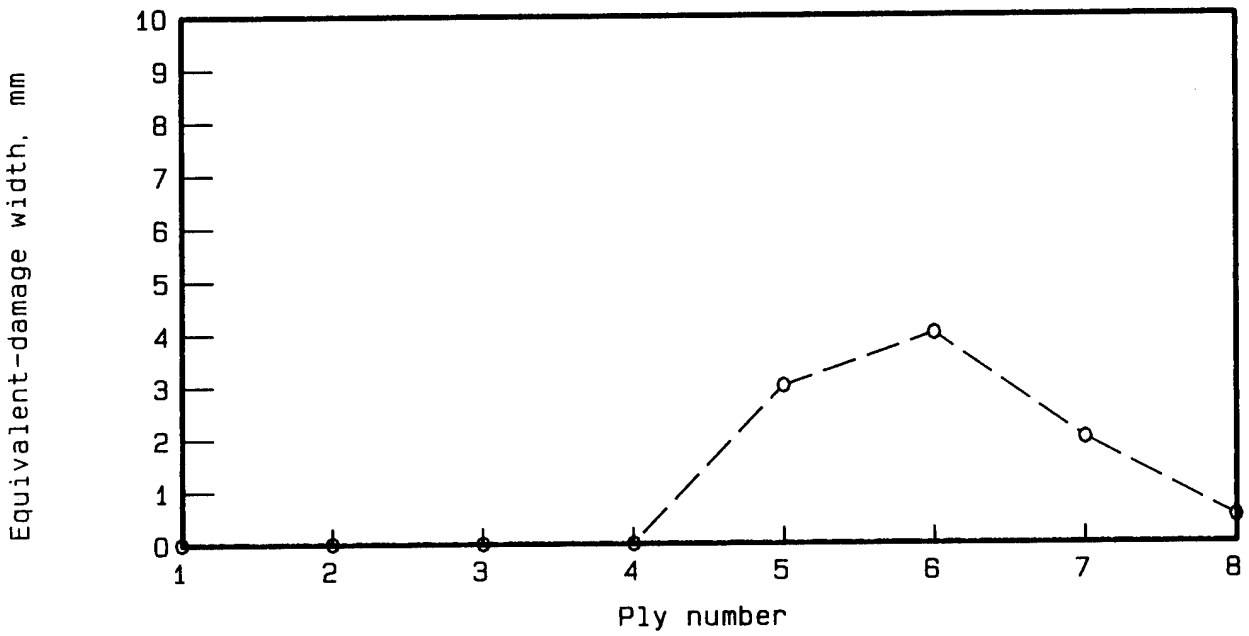

Figure 17.- Equivalent damage width for each ply of a plate loaded statically to a strain energy of 0.92 J.

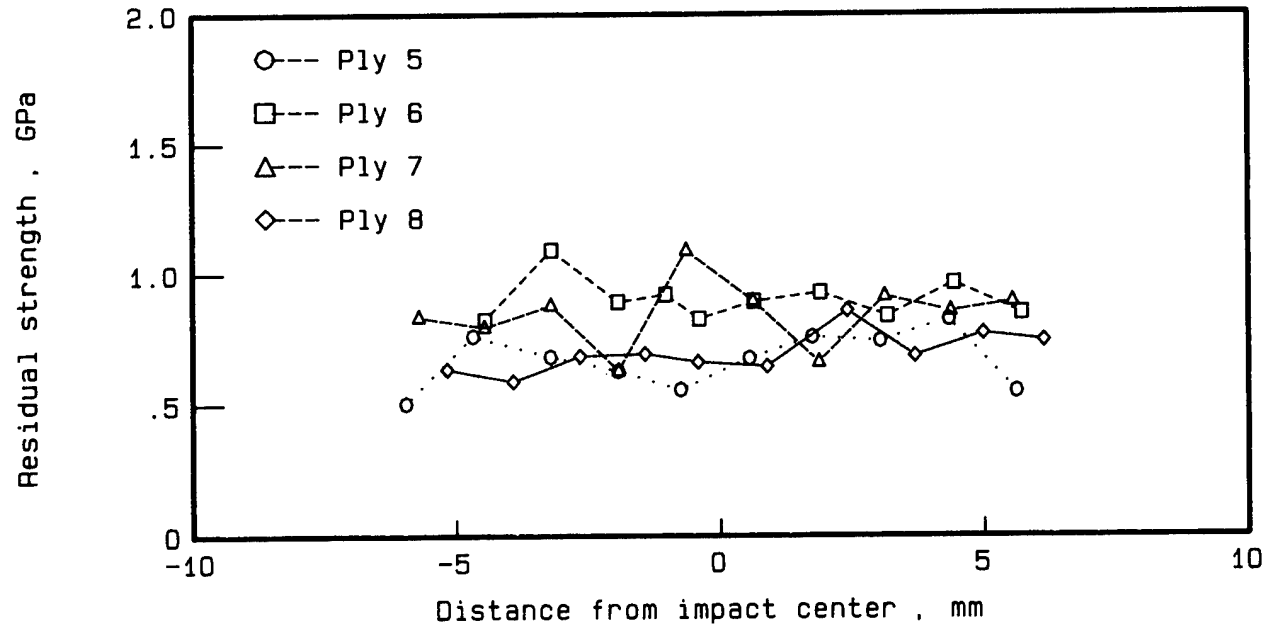

Figure 18.- Residual bundle strength for lower plies of a plate impacted at an energy of 0.61 J.

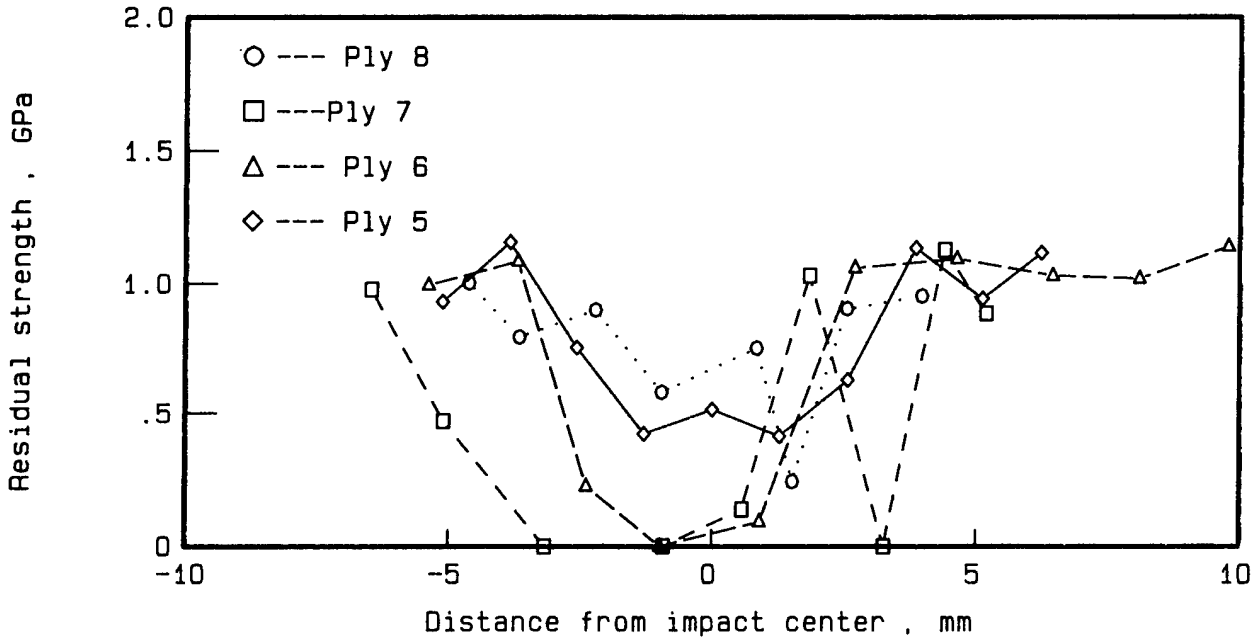

(a) Lower plies (5, 6, 7, and 8).

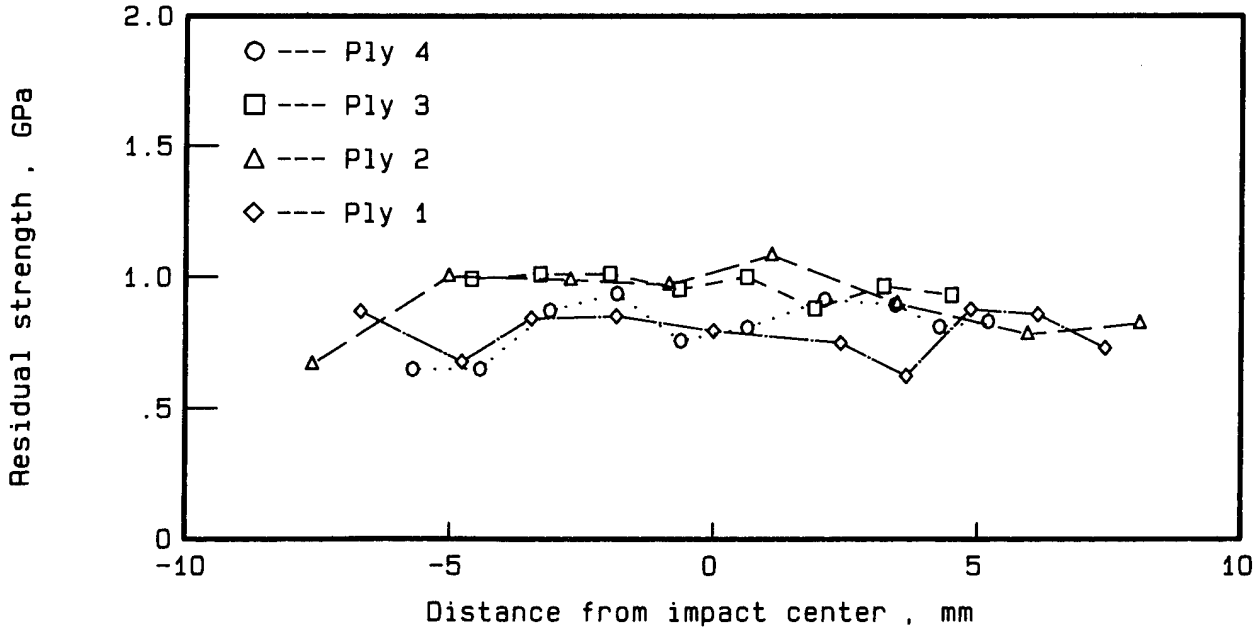

(b) Upper plies (1, 2, 3, and 4).

Figure 19.- Residual bundle strengths for all 8 plies of a plate impacted at an energy of 1.04 J.

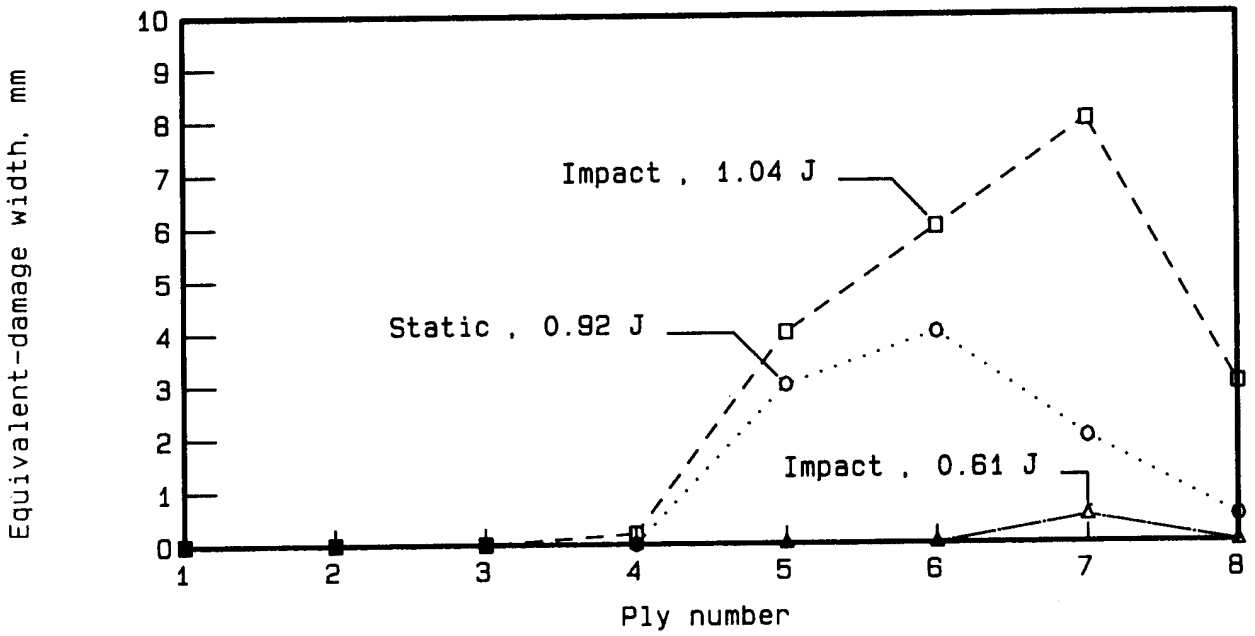

Figure 20.- Comparison of fiber damage distribution for three loading energy levels.

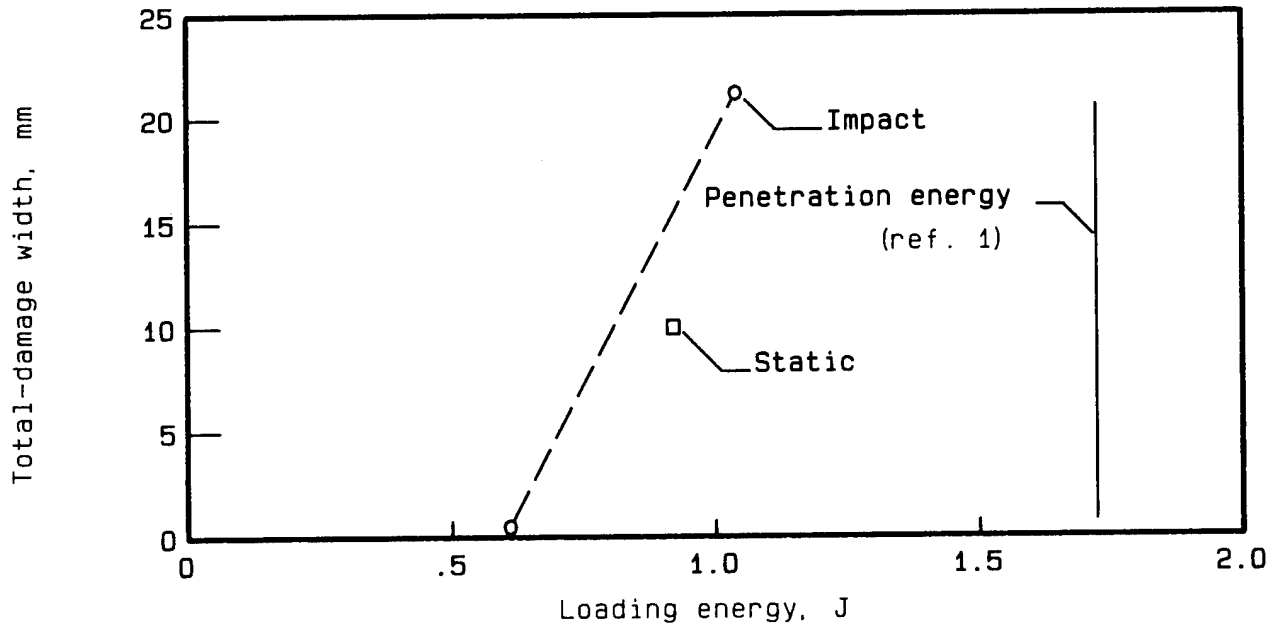

Figure 21.- Comparison of total fiber damage width for two impact tests and one static test.

1. Report No.	2. Government Accession No.	3. Recipient's Catalog No.
NASA TP-2152		

4. Title and Subtitle	5. Report Date
FAILURE MECHANICS IN LOW-VELOCITY IMPACTS ON THIN COMPOSITE PLATES	May 1983
	6. Performing Organization Code: 506-53-23-05

7. Author(s)	8. Performing Organization Report No.
Wolf Elber	L-15588
	10. Work Unit No.

9. Performing Organization Name and Address	11. Contract or Grant No.
NASA Langley Research Center Hampton, VA 23665	
	13. Type of Report and Period Covered: Technical Paper

12. Sponsoring Agency Name and Address	14. Sponsoring Agency Code
National Aeronautics and Space Administration Washington, DC 20546	

15. Supplementary Notes

16. Abstract

Eight-ply quasi-isotropic composite plates of Thornel® 300 graphite in Narmco® 5208 epoxy resin (T300/5208) were tested to establish the degree of equivalence between low-velocity impact and static testing. Both the deformation and failure mechanics under impact were representable by static indentation tests. Under low-velocity impacts such as tool drops, the dominant deformation mode of the plates was the first, or static, mode. Higher modes are excited on contact, but they decay significantly by the time the first-mode load reaches a maximum. The delamination patterns were observed by X-ray analysis. The areas of maximum delamination coincided with the areas of highest peel stresses. The extent of delamination was similar for static and impact tests. Fiber failure damage was established by tensile tests on small fiber bundles obtained by deplying test specimens. The onset of fiber damage was in internal plies near the lower surface of the plates. The distribution and amount of fiber damage was similar for impact and static tests.

17. Key Words (Suggested by Author(s))	18. Distribution Statement
Composites Test data Damage mechanisms Low-velocity impact	Unclassified - Unlimited Subject Category 24

19. Security Classif. (of this report)	20. Security Classif. (of this page)	21. No. of Pages	22. Price
Unclassified	Unclassified	25	A02

For sale by the National Technical Information Service, Springfield, Virginia 22161

NASA-Langley, 1983